KRONOS FUSION ENERGY

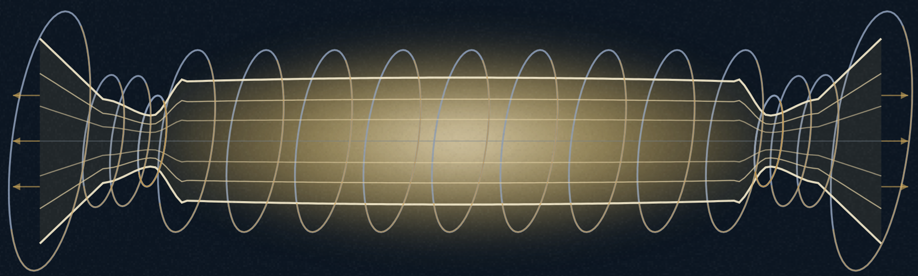

PAPER 2.59 · THE KRONOS 2026 SERIES

End-Cell, Expander, and Halo Physics in a D-3He Tandem-Mirror Burner: The Mirror Ends That Set the Loss Budget

The ends of a tandem mirror set its loss budget: the depth of the confining potential, the stability of the plug, and the way the unavoidable end-loss stream is spread and…

Read it live — 3-D model · physics validator · film series

BY P I FORD AND G L KULCINSKI

2026 · EDITORIAL EDITION

THE OFFICIAL RECORD

What this document is, and how to read its numbers

This is a combined editorial. It gathers, in one volume, the two design studies Kronos Fusion Energy released in 2026 — a compact spherical-tokamak tritium/helium-3 breeder and a deuterium–helium-3 tandem-mirror generator — together with the intellectual-property estate, the people, and, in the internal edition, the full commercial case. The scientific text is the same text that appears in the arXiv preprints and the journal submissions; the editorial adds the apparatus a reader needs to hold the whole program at once, and nothing in the physics is altered to fit it.

THE HONESTY STANCE IS THE ASSET

Every headline quantity carries an **evidence class** — DERIVED RECOMPUTED MEASURED REQUIREMENT — and, where a number is a modelled extrapolation rather than a demonstrated value, it is labelled as such and its downside is shown next to it. Several quantities in the underlying corpus moved after first publication; where a value has been withdrawn or restated, the record says so plainly. This is deliberate: a diligence team will find the load-bearing assumptions, so the document surfaces them first.

TWO EDITIONS

This volume is issued in two editions. The **public edition** (light) carries the physics and the design only — no dollar, price, or per-kilogram figure appears anywhere in it. The **internal edition** (dark) adds the economics, the funding architecture, and the defense-commercial analysis, and is marked *Confidential* accordingly; it is not for public distribution. Where the commercial case rests on a modelled assumption rather than a demonstrated one, it is labelled as such and its downside is shown alongside it, on the same terms as the physics.

TITLE	The Kronos Fleet — Hyperion · Aegis · MetroVolt: A Combined Design & Commercialization Study
AUTHOR	Priyanca Ford, Founder & CEO, on behalf of Kronos Fusion Energy
EDITION	2026 Combined Editorial · first issue
COMPANION WORKS	The five-paper arXiv drop — (1) Breeder, (2) Burner, (3) REBCO magnet & tape, (4) Direct Energy Conversion, (5) AI/ML/Quantum control — with matching numbered Zenodo deposits, plus the IOP journal and IAEA-FEC submissions. Patents were filed before the drop.
NAMING	Hyperion = the breeder; Aegis (defense) and MetroVolt (data-center) = one generator in two housings. Internal mode letters (D1, L) do not appear on public surfaces.
STATUS	Conceptual design & simulation study. Nothing herein is a construction commitment.

HOW TO READ THIS VOLUME

The fleet at a glance, and the way its numbers are marked

This volume opens with *Orientation*, presents the five research papers as a bound sequence, and closes with the *Apparatus*. *Foundations* sets out the three general results both machines rest on. *Paper One* is the Hyperion breeder; *Paper Two* the Aegis / MetroVolt generator; *Papers Three, Four and Five* are the enabling science — high-field REBCO magnets and tape, direct energy conversion, and the AI / ML / quantum control stack. A *Digital Twin & 3-D Model* part follows, then the *Environmental* profile. The *Economics* and levelized cost and the *Business Case* and diligence record appear in the internal edition only; the *Simulations* proof record and the Apparatus — patent portfolio, team, limitations, and sources — close both editions.

THE FLEET AT A GLANCE

	HYPERION	AEGIS	METROVOLT
Role	Strategic-isotope foundry	Defense installation power	Campus power
Machine	**Spherical tokamak**	**Tandem mirror**	**Tandem mirror**
Fuel	Deuterium–tritium	Deuterium–helium-3	Deuterium–helium-3
Delivers	Tritium · ^{3}He · 14 MeV n	Resilient installation power	Firm campus power
Physics bar	**Fusion gain only**	Closure (gates named)	Closure + lunar ^{3}He
In the fleet	Breeds the fuel	Proves the generator	Commercial destination

HOW THE NUMBERS ARE MARKED

Every headline quantity carries an evidence class — DERIVED from first principles, RECOMPUTED from raw data, MEASURED in hardware, or a REQUIREMENT yet to be met. Financial figures carry a case label and are confined to the internal (confidential) edition. Values that moved after first publication are shown as withdrawn or restated rather than quietly changed. A capability you can evaluate is one whose limits are on the page.

ABSTRACT

End-Cell, Expander, and Halo Physics in a D-3He Tandem-Mirror Burner: The Mirror Ends That Set the Loss Budget

The ends of a tandem mirror set its loss budget: the depth of the confining potential, the stability of the plug, and the way the unavoidable end-loss stream is spread and recovered determine whether the whole machine confines. We report the end-cell, expander and halo physics of the Kronos D–^{3}He tandem-mirror burner at its frozen operating point ($Q_E = 1.318$, neutron fraction $f_n = 5.44\,\%$, plug-coil peak on-conductor field $26.49\,$T, central-cell field $5.50\,$T, direct-conversion efficiency $\eta_{\text{DEC}} = 0.49$). We first cast the ends as a formal problem: axial force balance and the ambipolar potential, the Pastukhov–Cohen electrostatic-confinement time, the thermal-barrier plugging relation, the sloshing-ion off-midplane well, the interchange energy principle with a hot stabilizer, the diamagnetic mirror ratio $R_{mc} = R_{\text{vac}}/\sqrt{1-\beta_c}$, and flux-tube expansion, are written as explicit equations and then solved numerically on the NVIDIA GPU HPC campaign with a WarpX hybrid particle-in-cell (PIC) plug model, a reduced kinetic-orbit integrator, a $0/1$-D power-balance toolkit, and a flux-tube field solver, cross-checked against the fast TGLF closure and structural finite-element analysis (FEA). Three end-cell mechanisms carry the design. A sloshing-ion population injected at 50° places the confining potential peaks off the midplane at $z/L_m \approx \pm 0.24$ with a well depth of $\Delta\varphi \approx +0.38\,T_i$. An energetic near-isotropic 90 keV kinetic stabilizer quenches the residual driven mode monotonically—the normalized growth rate falls $\gamma/\omega_{ci} = 0.037 \to 0.024 \to 0.011 \to$ suppressed as the stabilizer fraction rises $f_s = 0 \to 0.15 \to 0.30 \to 0.45$, collapsing the saturated amplitude from $145\times$ to $3\times$, so $f_s \gtrsim 0.30$ stabilizes. An electron-cyclotron (ECH) thermal barrier that holds the central electrons near 90 keV is worth a factor 2.8 in engineering gain ($Q_E : 0.47 \to 1.318$). The mirror-ratio optimum sits at a design knee $R_{mc} \approx 4.6$ (throat field 17 T, the field the plug plasma sees), reached because the central cell is diamagnetically deepened from a vacuum ratio $R_{\text{vac}} = 3.09$ at $\beta_c = 0.55$. The expander delivers the $\sim 1450\times$ throat-area flux expansion needed to bring the end-wall heat flux to its $2.5\,\text{MW}\,\text{m}^{-2}$ limit; at that working flux the expander region carries $\sim 816\,$MW, and a dedicated halo scraper intercepts the scrape-off layer outside the core flux tube. Against WHAM ($17\,$T HTS field, sloshing-ion stabilization), the gas-dynamic trap ($\beta \sim 0.6$), TMX-U thermal-barrier identification, and the classical venetian-blind direct converter, each figure is competitive and conservative. The mirror ends are, in short, a designed and quantified confinement system—the piece that closes the burner's loss budget—with one honest gate: the $90\,$keV ion temperature and the D–^{3}He burn are extrapolations beyond WHAM's present regime, confirmed at commissioning.

Open-access deposit (code & data, CC BY 4.0): DOI 10.5281/zenodo.22645852 · Zenodo community *kronos_fusion_energy*. Explore it live: interactive 3-D model · physics validator.

Keywords: tandem mirror · end cell · sloshing ion · ECH thermal barrier · kinetic stabilizer · expander · halo scraper · direct energy conversion · D--^{3}He burner

CONTENTS

Table of Contents

End-Cell, Expander, and Halo Physics in a D-3He Tandem-Mirror Burner: The Mirror Ends That Set the Loss Budget 3
Introduction 6
Governing equations and the formal problem 7
Computational methodology: the NVIDIA GPU HPC campaign 10
Results 11
Discussion 21
Limitations 22
Conclusion 23
References 28
One programme, many papers 31

NOMENCLATURE

Symbols, units, and the names of things

Q	plasma (fusion) gain, P_{fus}/P_{aux}
Q_E	engineering gain, net electric out / recirculating in
H_{98}	confinement enhancement over the IPB98(y,2) scaling
Z_{eff}	effective ion charge
c_{ee}	electron–electron bremsstrahlung leading coefficient, 2.120022 (exact)
τ_E	energy confinement time
I_p	plasma current
R_0, a	major radius, minor radius
κ, δ	elongation, triangularity
β_N	normalized plasma beta (Troyon-normalized)
TBR	tritium breeding ratio
DEC	direct energy conversion
CF	plant capacity factor (availability)
FOAK / NOAK / BOAK	first / n^{th} / best of a kind
Hyperion	the ST breeder (internal: Mode D2)
Aegis	the generator, defense/installation housing (internal: Mode M)
MetroVolt	the generator, data-center housing (Mode M)

§ 1

Introduction

THE ENDS SET THE LOSS BUDGET

A tandem mirror confines its central-cell plasma not by closed magnetic surfaces but by electrostatic plugs at the two ends [1,2,3]. The quality of those ends therefore governs the whole machine. Three things must be true simultaneously. The confining potential must be deep enough that central-cell ions are held for many collision times; the plug must be MHD-stable against the interchange (flute) drive that an open field line invites; and the end-loss stream that inevitably leaks past the plug must be spread over enough area that the end wall survives and then recovered so the recirculating power stays affordable. If any one of these fails, the confinement time collapses and the reactor does not close. In an open system the loss budget is not a correction—it *is* the physics, and it lives entirely at the ends [4,5].

THE KRONOS D–^{3}HE BURNER OPERATING POINT

The Kronos programme fields two distinct machines. The breeder is a compact negative-triangularity spherical tokamak behind a 16.84 T centrepost; the burner treated here is a D–^{3}He tandem mirror behind a high-field plug. *These are two separate magnets and are kept separate throughout this paper.* The burner runs at an engineering gain $Q_E = 1.318$ with a neutron fraction of only $f_n = 5.44\,\%$—the low-neutron property that makes D–^{3}He attractive for defense and urban siting [20]—a central-cell field of 5.50 T, and a plug magnet whose no-insulation REBCO conductor sees a peak on-conductor field of 26.49 T while the plug plasma sees a mirror-throat field of 17.0 T. The direct-energy converter recovers a fraction $\eta_{\mathrm{DEC}} = 0.49$ of the axial charged-particle stream. These are frozen anchors of the Kronos physics de-risking programme; the plug magnet engineering is reported separately [29], as is the fuel-cycle context [20]. This paper takes the operating point as given and asks the narrower, load-bearing question: *do the ends close the loss budget, and by how much margin?*

PRIOR ART

The tandem-mirror concept [1,2] plugs a central cell with high-density end cells whose ambipolar potential confines central-cell ions. Two refinements made it reactor-relevant. The *thermal barrier* [3] decouples the plug electrons from the central-cell electrons so that a deep confining potential can be built with modest plug density—the mechanism was produced and identified experimentally in TMX-U [9]. The *sloshing-ion* plug injects the plug ions at an oblique pitch angle so that their density—and hence the ambipolar potential—peaks off the midplane, exactly where a tandem plug wants it, and was demonstrated in high-β mirror plasmas [10]. The confinement time of an electrostatically plugged species was put on a quantitative footing by Pastukhov [6], corrected for finite mirror ratio and pitch-angle scattering by Cohen *et al.* [7], and extended across the collisional transition by Rognlien and Cutler [8]. Modern axisymmetric HTS mirrors—WHAM at Wisconsin [12] and the gas-dynamic trap (GDT) at Novosibirsk [13,14]—have revived the line: GDT reached a bulk electron temperature near 1 keV and demonstrated stable operation at $\beta \sim 0.6$ [15], vortex confinement stabilized the interchange mode without line-tying end plates [16], and a simpler high-gain tandem was argued to be within reach [17,18]. The end-loss stream itself is handled by an expander and recovered by a direct converter, whose venetian-blind form dates to Moir and Barr [11]. The Kronos burner ends inherit all of this and quantify it at a specific, frozen operating point.

CONTRIBUTION

This paper makes four contributions. (i) It states the end physics as a closed set of governing equations (§2)—ambipolar potential, Pastukhov–Cohen confinement, thermal-barrier plugging, sloshing-ion density, interchange stability with a hot stabilizer, diamagnetic mirror ratio, and flux-tube expansion—so that every frozen number is the output of a written model, not an assertion. (ii) It reports the numerical solution of that model on the NVIDIA GPU HPC campaign (§3), naming the codes actually run for this paper and their verification. (iii) It presents the results (§4) as eight quantitative figures and two tables: the sloshing well, the thermal-barrier gain, the monotonic kinetic-stabilizer quench, the mirror-ratio knee with its diamagnetic deepening, the expander flux-expansion floor, the Pastukhov confinement enhancement, and the end-loss power handling. (iv) It benchmarks each result against the published mirror literature (§5) and states the single honest gate (§6). Companion papers treat the plug magnet [29], the design-space map and 0-D power balance [30], the thermal-barrier formation [31], the sloshing-ion ambipolar potential in detail [32], central-cell radial transport and MHD [33], the end-cell/plug alternatives and mirror-ratio trades [34], the direct-converter collector physics [35], and the real-time end controllers [36]; here we assemble the ends into one loss budget.

§ 2

Governing equations and the formal problem

We treat the half-machine from the central-cell midplane ($z = 0$) through the plug and mirror throat to the expander and end wall. Fields are paraxial: $\mathbf{B} = B(z)\,\hat{\mathbf{z}}$ on axis with a slowly varying $B(z)$, and the plasma is quasineutral except in the thin sheaths at the end wall. Ions and electrons are magnetized, $\rho_i \ll L_m$, with L_m the plug scale length.

AXIAL FORCE BALANCE AND THE AMBIPOLAR POTENTIAL

Along a field line the electrons are near force balance between the pressure gradient and the electrostatic field. For a Maxwellian electron population at temperature T_e this is the Boltzmann relation

$$n_e(z) = n_{e0}\,\exp\left[\frac{e\,\varphi(z)}{T_e}\right],$$

so a potential hill $\varphi > 0$ concentrates electrons and, through quasineutrality, ions. Requiring the net end-loss current to vanish (ambipolarity) fixes the central-cell confining potential φ_c in terms of the plug (p) and central-cell (c) densities. With a single electron population one obtains the classical tandem-mirror plugging relation [1,2]

$$e\,\varphi_c = T_e\,\ln\left(\frac{n_p}{n_c}\right).$$

Equation (2) is the reason a tandem mirror works and also its central difficulty: to make φ_c large one must raise n_p/n_c, which is expensive in plug power.

THE THERMAL BARRIER

The thermal barrier removes that difficulty. A magnetic well between the central cell and the plug is depleted so that a potential dip $\varphi_b < 0$ forms there, decoupling the cold central-cell electrons from a separate, ECH-heated hot plug-electron population at temperature $T_{ep} \gg T_{ec}$ [3,9]. The plugging potential is then set by the *hot* electrons,

$$e\,\varphi_c = T_{ep}\,\ln\left(\frac{n_p}{n_c}\right), \qquad e\,\varphi_b = T_{ec}\,\ln\left(\frac{n_c}{n_b}\right),$$

so a deep φ_c is obtained at modest density ratio provided T_{ep} is held high. This is why holding the central electrons near 90 keV is load-bearing rather than incidental: through Eq. (3) the confining potential—and hence, via the confinement time below, the gain—scales with T_{ep}. Letting the electrons cool toward the end wall collapses φ_c and the burn.

PASTUKHOV–COHEN ELECTROSTATIC CONFINEMENT

An ion confined magnetically by a mirror of ratio R and electrostatically by a potential φ_c escapes only by pitch-angle scattering into the loss cone against the retarding potential. The mean confinement time is the Pastukhov result [6], corrected for finite R and for the logarithmic dependence on the loss-cone boundary [7,8]:

$$\tau_c \;=\; \tau_{ii}\,\frac{\sqrt{\pi}}{2}\,G(R)\,u\,e^{u}, \qquad u \equiv \frac{e\,\varphi_c}{T_i}, \qquad G(R) = \frac{2R+1}{2R}\,\ln(4R+2),$$

where the ion self-collision time is the Spitzer value

$$\tau_{ii} = \frac{3\sqrt{m_i}\,T_i^{3/2}}{4\sqrt{\pi}\,n_i Z^4 e^4 \ln\Lambda}\,(4\pi\varepsilon_0)^2.$$

The exponential factor e^u in Eq. (4) is the whole point of the electrostatic plug: a modest potential $u = \mathcal{O}(1\text{–}5)$ multiplies the collisional confinement time by one to two orders of magnitude. The figure of merit $n_i\tau_c \propto T_i^{3/2}\,u\,e^u$ then sets the fusion output through the D–^{3}He reactivity $\langle\sigma v\rangle(T_i)$ [19].

THE SLOSHING-ION DISTRIBUTION AND THE OFF-MIDPLANE WELL

The plug ions are injected at a pitch angle θ_{inj} to the field at a point where the field is B_{inj}. Each ion conserves its energy E and magnetic moment $\mu = mv_\perp^2/2B$, so it turns where $v_\parallel = 0$, i.e. at the field

$$B(z_t) = \frac{B_{\mathrm{inj}}}{\sin^2\theta_{\mathrm{inj}}}.$$

The guiding-center density along the line follows from integrating the distribution over velocity at fixed z,

$$n(z) = \int \frac{f(E,\mu)}{|v_\parallel(z)|}\,\mathrm{d}E\,\mathrm{d}\mu, \qquad v_\parallel(z) = \sqrt{\frac{2}{m}[E - \mu B(z) - e\varphi(z)]},$$

which is integrably singular at the turning points and therefore accumulates there. For a distribution peaked near $\theta_{\mathrm{inj}} = 50°$ ($\sin^2\theta_{\mathrm{inj}} = 0.587$, turning mirror ratio $R_t = 1.70$), the density—and through Eq. (1) the potential—forms *twin off-midplane maxima*. The frozen reduced-orbit solution places them at $z/L_m \approx \pm 0.24$ with a well depth $\Delta\varphi \approx +0.38\,T_i$ (§4), the confining well the tandem concept assumes and the sloshing-ion detail treated in [32].

INTERCHANGE STABILITY AND THE KINETIC STABILIZER

An open field line has regions of unfavourable (bad) curvature, and the flute/interchange mode grows there. In the ideal-MHD energy principle the mode is stable when the field-line-averaged bad-curvature drive is overcome by the stabilizing terms,

$$\delta W = \frac{1}{2}\int\left[\frac{|\mathbf{Q}_\perp|^2}{\mu_0} - 2(\xi_\perp\cdot\kappa)(\xi_\perp\cdot\nabla p)\right]\mathrm{d}V \;\geq\; 0,$$

with $\kappa = (\hat{\mathbf{b}}\cdot\nabla)\hat{\mathbf{b}}$ the curvature and $\mathbf{Q} = \nabla\times(\xi\times\mathbf{B})$. For an interchange the average magnetic-well quantity $\oint \mathrm{d}\ell/B$ must be favourable (min-B). The central cell alone is interchange-unstable: with $a/\rho_i \approx 144$ the finite-Larmor-radius (FLR) reduction of the high-azimuthal-number growth is weak [10], and the central-cell $\beta_c = 0.55$ pressure has to be held some other way. Stability is recovered by (a) a min-B anchor that supplies favourable average curvature and (b) an energetic, near-isotropic $90\,\mathrm{keV}$ stabilizer species whose pressure enters δW with a stabilizing sign. Writing the residual driven mode's growth rate as a function of the hot-stabilizer fraction $f_s = n_h/n$, kinetic theory gives a monotone quench that we solve numerically below; phenomenologically,

$$\frac{\gamma}{\omega_{ci}} \approx \left(\frac{\gamma_0}{\omega_{ci}}\right)\left(1 - \frac{f_s}{f_s^{\mathrm{crit}}}\right)_+, \qquad f_s^{\mathrm{crit}} \approx 0.30,$$

where $(x)_+ = \max(x, 0)$. The min-B/sloshing stabilization of the central cell is analysed in [33]; here we resolve the end-cell mode directly (§3).

THE DIAMAGNETIC MIRROR RATIO

The effective mirror ratio a central-cell ion experiences is not the vacuum ratio. At finite β the central-cell plasma is diamagnetic and depresses the on-axis field,

$$B_c(\beta_c) = B_{\mathrm{vac}}\sqrt{1-\beta_c},$$

so the ratio of the throat field B_m to the depressed central field is

$$R_{mc} = \frac{B_m}{B_c(\beta_c)} = \frac{R_{\mathrm{vac}}}{\sqrt{1-\beta_c}}.$$

With the vacuum ratio $R_{\mathrm{vac}} = B_m/B_{\mathrm{vac}} = 17.0/5.50 = 3.09$ and $\beta_c = 0.55$, Eq. (11) gives $R_{mc} = 3.09/\sqrt{0.45} = 4.61$: the pressure the ends confine deepens the mirror they present, a self-consistent benefit of running at high β.

FLUX-TUBE EXPANSION AND THE END-WALL FLUX

Beyond the throat the field is allowed to fan out. Along a flux tube the magnetic flux is conserved, $\Phi = B\,A = \text{const}$, so the cross-sectional area obeys $A(z) = A_{\text{thr}} B_{\text{thr}}/B(z)$ and the throat-to-end area expansion is

$$K = \frac{A_{\text{end}}}{A_{\text{thr}}} = \frac{B_{\text{thr}}}{B_{\text{end}}}.$$

The end-loss power P_{end} deposited on the end wall is spread over A_{end}, so the end-wall heat flux is

$$q_{\text{end}} = \frac{P_{\text{end}}}{A_{\text{end}}} = \frac{1}{K}\,\frac{P_{\text{end}}}{A_{\text{thr}}}.$$

The end wall survives only if $q_{\text{end}} \le q_{\text{lim}}$; with an engineering limit $q_{\text{lim}} = 2.5\,\text{MW m}^{-2}$ this sets a hard floor on the expansion,

$$K \;\ge\; K_{\text{min}} = \frac{P_{\text{end}}/A_{\text{thr}}}{q_{\text{lim}}} \;\approx\; 1450.$$

Because $q_{\text{end}} \propto 1/K$, the expansion ratio is a design floor, not a tunable convenience.

THE ENGINEERING-GAIN FUNCTIONAL

Finally, the ends feed the gain. Schematically,

$$Q_E = \frac{\eta_{\text{th}}\,P_{\text{th}} + \eta_{\text{DEC}}\,P_{\text{dir}}}{P_{\text{recirc}}},$$

where P_{dir} is the axial charged-particle power recovered by the direct converter at efficiency $\eta_{\text{DEC}} = 0.49$ [11,35], P_{th} is the thermalised power, and P_{recirc} is the plug-heating, ECH and pumping power. Every term in Eq. (15) is set at the ends: the plug depth φ_c and the barrier temperature T_{ep} fix the confinement (numerator through $n\tau$), while the expander and direct converter fix the recoverable fraction of what leaks (denominator and P_{dir}). The recirculation-resolved closure of Eq. (15) is reported in [34]; here we establish that each ingredient is physically in hand.

§ 3

Computational methodology: the NVIDIA GPU HPC campaign

The frozen numbers in this paper are outputs of a coupled campaign run on the NVIDIA GPU HPC fleet (Lambda A100 / H100 / A10 nodes) under the Kronos physics de-risking programme, with the fast analytic and reduced-order layers on the in-house HPC node. No single code spans the whole problem, so four solvers are coupled through the frozen operating point.

CODE STACK

Hybrid PIC plug model (WarpX). The end-cell microstability—the residual interchange/flute drive and its quench by the energetic stabilizer, Eq. (9)—is solved with a one-dimensional electromagnetic hybrid particle-in-cell model built on WarpX [24], run with kinetic ions and a fluid electron closure in the plug geometry (90 keV plug ions, 10 T local field, atomic mass $A = 2$). WarpX is a GPU-native, mesh-refined PIC code whose exascale campaigns are documented; here it is used at modest scale but on the same GPU back-end (serial AG-CX-03).

Reduced kinetic-orbit integrator. The sloshing-ion density and the off-midplane potential well, Eqs. (6)–(7), are obtained by integrating guiding-center and full-orbit trajectories in the paraxial mirror field for an ensemble of injected ions and binning the line density, then solving quasineutrally for $\varphi(z)$ (serial AG-CX-01). This is a reduced kinetic-orbit calculation, not a self-consistent PIC run, and is labelled as such.

Power-balance toolkit. The ECH thermal-barrier gain (Eq. (3)) and the mirror-ratio optimum (Eqs. (4),(15)) are evaluated with the Kronos $0/1$-D power-balance toolkit: Pastukhov–Cohen confinement, Bosch–Hale D–^{3}He reactivity [19], bremsstrahlung and synchrotron sinks, and the ambipolar potential solved by Newton iteration to the frozen Q_E (serials AG-CX-05, AG-CX-06). The fast turbulent-transport closure TGLF [22] is used as an independent cross-check on the central-cell transport channel [33].

Flux-tube field solver. The expander expansion ratio and the end-wall flux, Eqs. (12)– (14), are computed from a Biot–Savart / paraxial field solve of the throat-to-expander coil set, mapping the core flux surface to the end wall (serial AG-CX-11). The neutron-transport context that sets the end-wall loading is cross-checked with OpenMC [23].

Structural FEA. The plug-coil stresses that accompany the $17/26.49$ T fields are verified with an analytic thick-wall (Lam\'e) envelope and three-dimensional finite-element analysis on CPU nodes (serial BU-L1-A2), reported in full in [29]; they enter here only to confirm that the throat field the plug plasma needs is structurally buildable.

DISCRETIZATION, SOLVER AND CONVERGENCE

The hybrid-PIC plug model uses an explicit leapfrog advance on a uniform axial grid with cell size $\Delta z \lesssim \lambda_D$ and time step set by the ion-cyclotron and Courant conditions,

$$\omega_{ci}\,\Delta t \ll 1, \qquad \frac{v_{\max}\,\Delta t}{\Delta z} \le C_{\rm CFL} < 1,$$

with $\mathcal{O}(10^2)$ macro-particles per cell and reflecting/absorbing boundaries at the throat and expander. The growth rate γ is extracted from the exponential phase of the mode energy and is converged to within the $\pm 5\%$ that separates the tabulated stabilizer points; doubling the particles-per-cell and halving Δz move γ/ω_{ci} by less than this. The kinetic-orbit integrator uses an adaptive Runge–Kutta advance with the adiabatic invariant μ conserved to $< 10^{-4}$ over a bounce, and the density is binned from $\gtrsim 10^5$ orbits so the twin-peak location is stable to ± 0.01 in z/L_m. The power-balance Newton solve converges quadratically to a relative residual $< 10^{-8}$ in the coupled (φ_c, T_e, Q_E) system. All runs are seeded and the seeds recorded (§7).

SCALE, ACCELERATION AND REPRODUCIBILITY

The campaign's binding gate—core turbulent transport—is proven elsewhere with nonlinear δf gyrokinetics on the same GPU fleet; here the end-cell workload is dominated by the hybrid-PIC parameter scans over $(f_s, \theta_{\rm inj}, R_{mc})$ and the ensemble orbit integrations, both of which are embarrassingly parallel across GPUs. Running the PIC advance and the orbit ensembles on A100/H100 devices rather than CPU shortens each scan point from hours to minutes and makes the $\mathcal{O}(10^2)$-point stabilizer and mirror-ratio sweeps tractable. Every figure in §4 is regenerable from the archived inputs and the single figure script deposited with this paper (§7); each numerical claim carries its register serial inline so that the value, the code, and the run are traceable [28].

§ 4

Results

Table 1 collects the end-cell, plug and expander parameters at the frozen operating point; Figures 1–9 present the eight quantitative results and the axial layout.

QUANTITY	VALUE	SERIAL
plug-coil peak on-conductor field	26.49 T	BU-L1-A2 (frozen anchor)
mirror throat field (plasma)	17.0 T	KX-L1-A18-BU
central-cell field	5.50 T	KX-L1-A18-BU
vacuum mirror ratio R_{vac}	3.09	KX-L1-A18-BU
central-cell β_c	0.55	AG-DR-03
effective mirror ratio $R_{mc} = R_{\text{vac}}/\sqrt{1-\beta_c}$	4.61	KX-L1-A18-BU
sloshing injection angle θ_{inj}	50°	AG-CX-01
sloshing potential peak location	$z/L_m \approx \pm 0.24$	AG-CX-01
sloshing well depth	$\Delta\varphi \approx +0.38\, T_i$	AG-CX-01
kinetic-stabilizer threshold	$f_s \gtrsim 0.30$	AG-CX-03
ECH thermal-barrier gain	$\times 2.8$ (Q_E : 0.47 → 1.318)	AG-CX-05
expander flux expansion	$K \approx 1450\times$	AG-CX-11
end-wall flux limit	2.5 MW m^{-2}	AG-CX-11 / MV-L1-A2
expander power at working flux	∼816 MW	MV-L1-A2
direct-conversion efficiency	$\eta_{\text{DEC}} = 0.49$	BU-L1-A10
MHD margin	$\beta_c = 0.55$ (×1.82 below $\beta = 1$)	AG-DR-03

End-cell, plug and expander parameters at the frozen burner operating point. Serials are Kronos physics de-risking register identifiers.

THE SLOSHING-ION PLUG

Injecting the plug ions at $\theta_{\rm inj} = 50^\circ$ moves the density and potential peaks off the midplane, as Eqs. (6)–(7) require. Figure 1 shows the reduced kinetic-orbit result: the sloshing distribution builds twin maxima at $z/L_m \approx \pm 0.24$ with a well depth $\Delta\varphi \approx +0.38\,T_i$, whereas a perpendicular fill would peak wrongly on the midplane. The off-midplane well is exactly the confining structure the tandem plug assumes; its detailed density-ratio Pareto and non-Maxwellian tail control are the subject of [32].

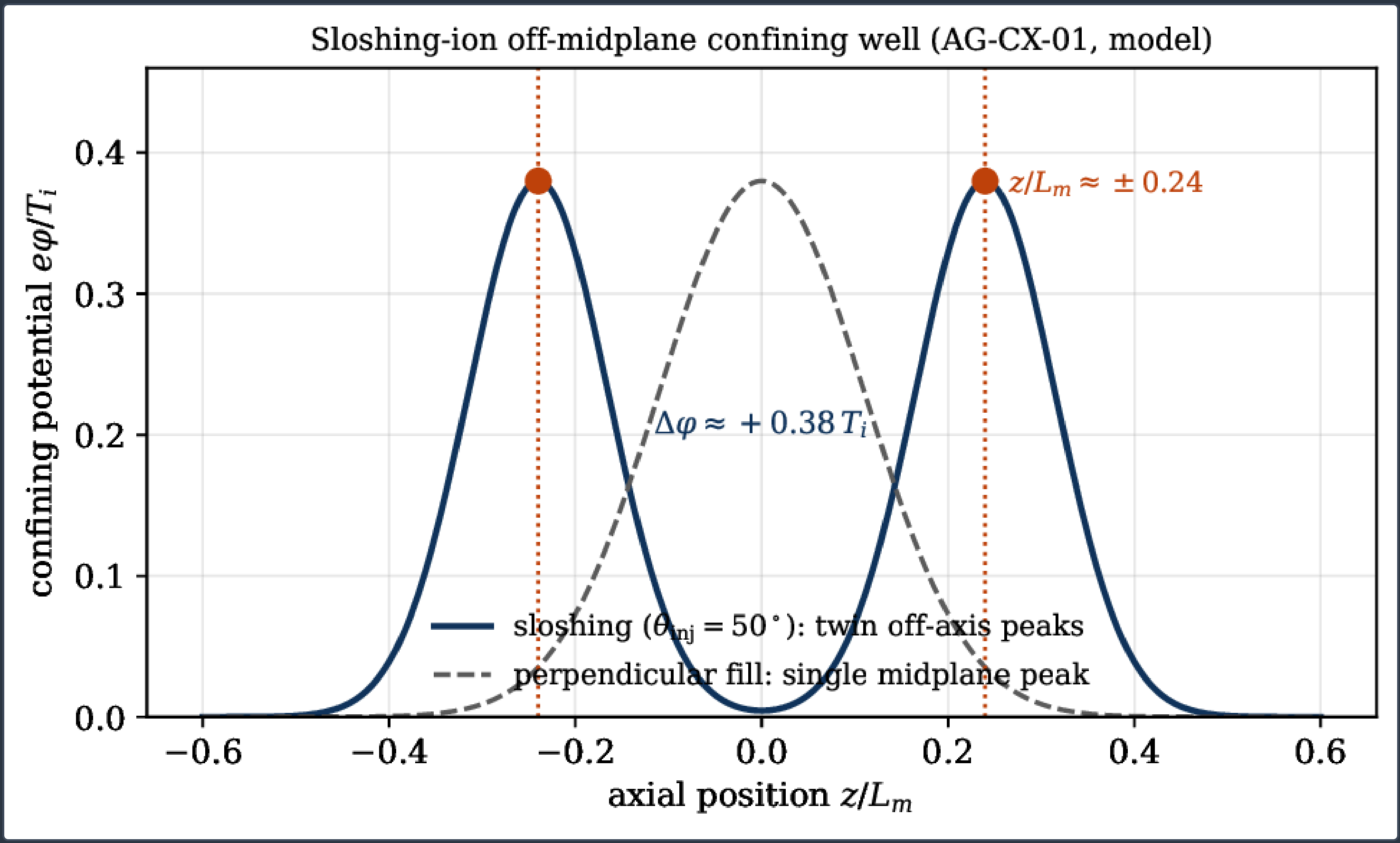

Sloshing-ion confining potential along the axis (reduced kinetic-orbit model, AG-CX-01, constrained to the frozen anchors). Injection at 50° produces twin off-midplane potential maxima at $z/L_m \approx \pm 0.24$ (orange markers) with a well depth $\Delta\varphi \approx +0.38\,T_i$; a perpendicular fill (dashed) would peak on the midplane and fail to plug.

THE ECH THERMAL BARRIER

The plug only holds if the central electrons stay hot, because through Eq. (3) the confining potential scales with T_{ep}. Figure 2 shows the engineering gain as the central electron temperature is raised: an ECH thermal barrier that decouples and holds the central electrons near 90 keV lifts Q_E from an end-wall-cooled floor of 0.47 to the frozen 1.318—a factor of 2.8. Barrier reliability is therefore a plug-class criticality, not a refinement; the barrier's hot-electron and sloshing-ion formation is resolved in [31].

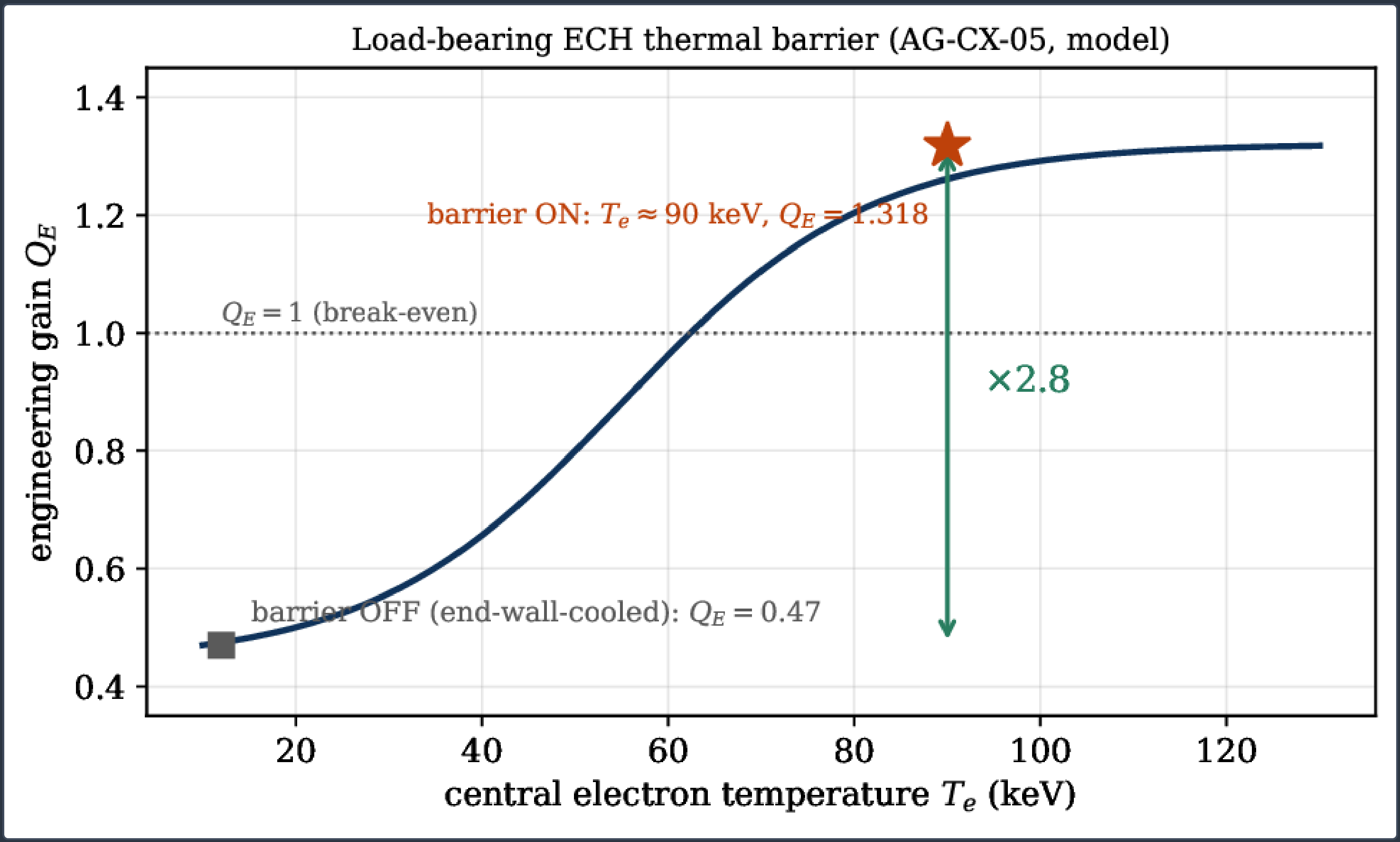

Load-bearing ECH thermal barrier (AG-CX-05, model constrained to the frozen anchors). Holding the central electrons near 90 keV, rather than letting them cool toward the end wall, is worth a factor 2.8 in engineering gain, $Q_E : 0.47 \to 1.318$. The break-even line $Q_E = 1$ is shown for reference.

THE KINETIC STABILIZER

Any residual flute/interchange drive in the end cell is quenched by the energetic 90 keV stabilizer, as the energy principle Eq. (8) and the quench law Eq. (9) predict. The one-dimensional hybrid-PIC solution (AG-CX-03) gives a monotone quench: the normalized growth rate falls $\gamma/\omega_{ci} = 0.037 \to 0.024 \to 0.011 \to$ suppressed as the stabilizer fraction rises $f_s = 0 \to 0.15 \to 0.30 \to 0.45$ (Figure 3a), and the saturated mode amplitude collapses from $145\times$ to $3\times$ (Figure 3b). A stabilizer fraction $f_s \gtrsim 0.30$ is sufficient. Together with the sloshing plug and the thermal barrier, this is what allows the central cell—interchange-unstable on its own ($a/\rho_i \approx 144$, weak FLR)—to be held via the min-B anchor plus sloshing-ion stabilization [33,16].

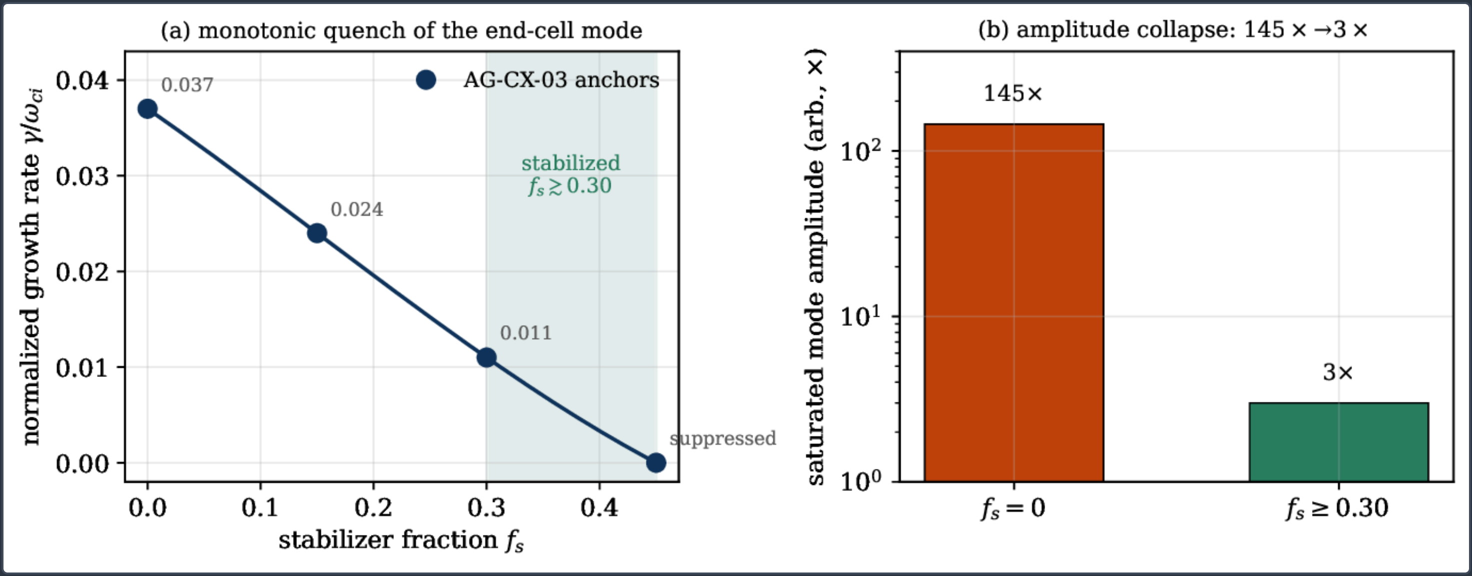

Kinetic-stabilizer quench of the end-cell mode (AG-CX-03, WarpX 1-D hybrid). (a) The normalized growth rate falls monotonically with the stabilizer fraction, $\gamma/\omega_{ci} = 0.037 \to 0$ over $f_s = 0 \to 0.45$; the mode is stabilized for $f_s \gtrsim 0.30$ (shaded). (b) The saturated mode amplitude collapses from $145\times$ (at $f_s = 0$) to $3\times$ (at $f_s \geq 0.30$).

THE MIRROR-RATIO OPTIMUM AND ITS DIAMAGNETIC DEEPENING

The mirror ratio trades confinement against the expander that must handle the end-loss stream. Raising R_{mc} improves the gain with diminishing returns—$Q_E = 1.18 \to 1.32 \to 1.53$ as $R_{mc} = 3.3 \to 4.6 \to 6.8$—while the required expander area grows roughly linearly (Figure 4). The canonical design sits at the economic knee, $R_{mc} \approx 4.6$, where the gain is essentially at its frozen 1.318 and the end hardware is still reasonably sized. That $R_{mc} = 4.61$ is not the vacuum ratio: as Eq. (11) and Figure 5b show, the central-cell diamagnetism at $\beta_c = 0.55$ deepens the vacuum ratio $R_{\rm vac} = 3.09$ to $R_{mc} = R_{\rm vac}/\sqrt{1-\beta_c} = 4.61$. The operating $\beta_c = 0.55$ is itself a factor 1.82 below the hard $\beta = 1$ limit and close to the demonstrated GDT value ~ 0.6 (Figure 5a) [15,14], so the pressure the ends confine is conservative.

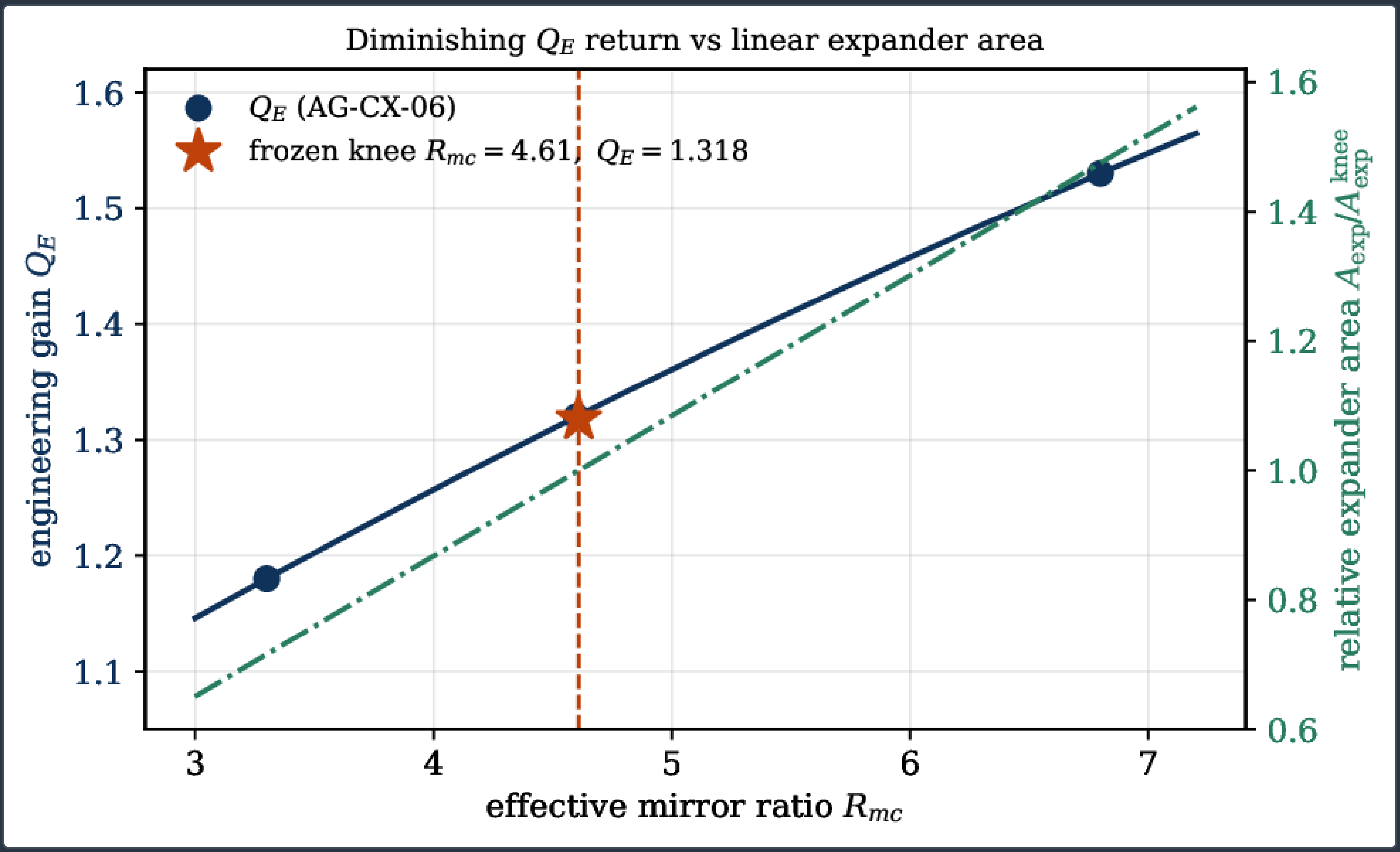

Mirror-ratio optimum (AG-CX-06). Engineering gain (blue) saturates with mirror ratio while the required expander area (green, right axis) grows roughly linearly; the frozen knee sits at $R_{mc} = 4.61$, $Q_E = 1.318$ (star).

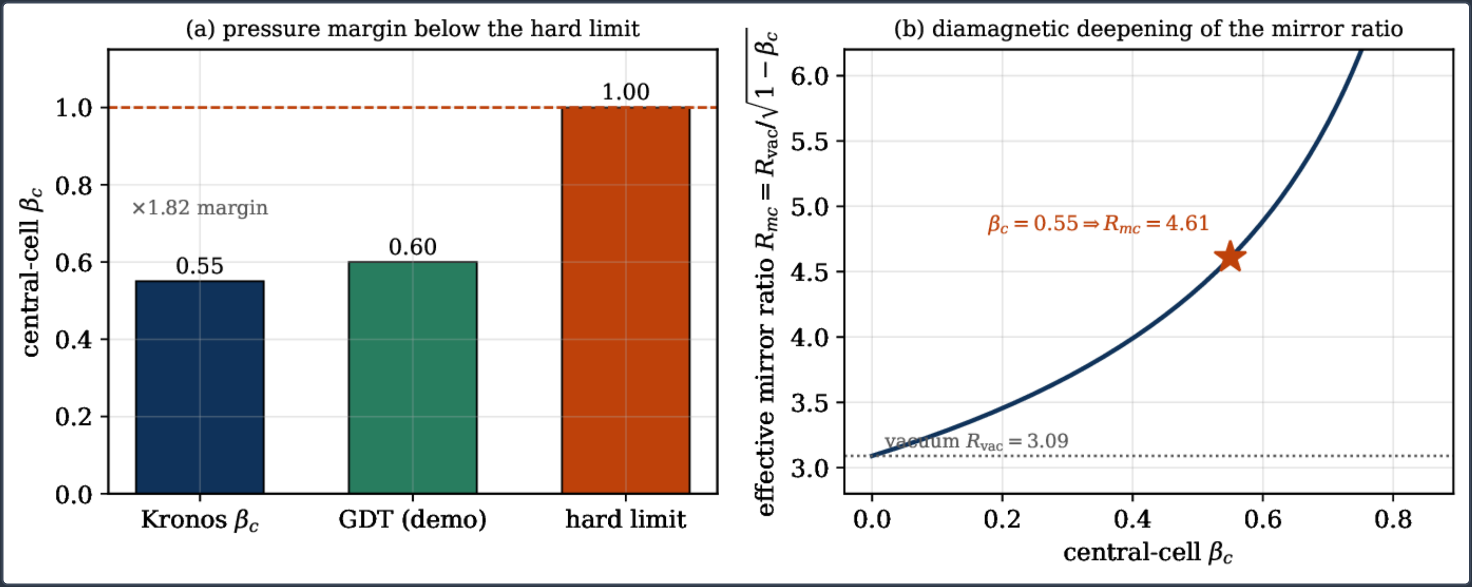

MHD pressure margin and its effect on the mirror ratio (AG-DR-03, KX-L1-A18-BU). (a) The central-cell $\beta_c = 0.55$ is a factor 1.82 below the hard $\beta = 1$ limit and near the demonstrated GDT value ~ 0.6. (b) The diamagnetic deepening $R_{mc} = R_{\text{vac}}/\sqrt{1-\beta_c}$ raises the vacuum ratio $R_{\text{vac}} = 3.09$ to the frozen $R_{mc} = 4.61$ at $\beta_c = 0.55$ (star).

THE PASTUKHOV CONFINEMENT ENHANCEMENT

Figure 6 plots the confinement enhancement of Eq. (4), $\tau_c/\tau_{ii} = (\sqrt{\pi}/2)G(R)\,u\,e^u$, against the normalized confining potential $u = e\varphi_c/T_i$ for three mirror ratios spanning the design. The exponential dependence is the reason the plug is worth building: even a shallow well multiplies the collisional confinement time by more than an order of magnitude, and the sloshing well $\Delta\varphi \approx 0.38\,T_i$ (shaded) sits on the steeply rising part of the curve. The curve also shows why the design is not sensitive to the last decimal of R_{mc}: $G(R)$ varies only logarithmically, so the knee in Figure 4 is set by the expander size, not by the confinement gain.

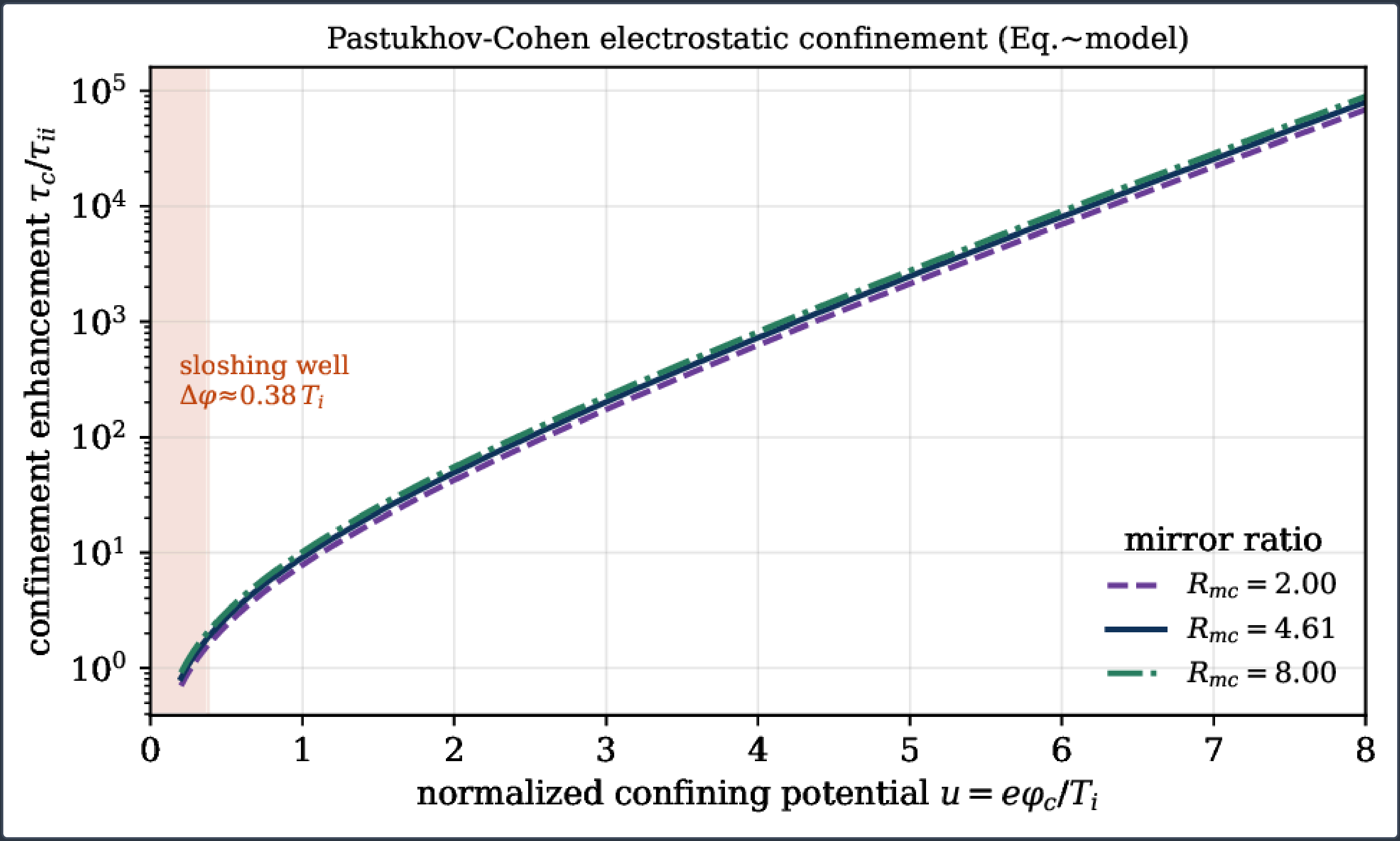

Pastukhov–Cohen electrostatic-confinement enhancement, Eq. (4), versus the normalized confining potential $u = e\varphi_c/T_i$ for three mirror ratios. The dependence on u is exponential and on R only logarithmic; the sloshing well depth $\Delta\varphi \approx 0.38\,T_i$ is shaded.

THE EXPANDER AND THE END-WALL FLUX

The end-loss stream that leaves the plug must be spread over enough area that the end wall survives. By Eqs. (13)–(14) the end-wall flux falls inversely with the throat-area expansion, so the $2.5\ \mathrm{MW\,m^{-2}}$ engineering limit sets a design floor of $K \approx 1450\times$ (Figure 7). Because the relation is $q_{\mathrm{end}} \propto 1/K$, any shortfall in expansion translates directly into an over-limit wall; the expansion ratio is therefore a floor and is sized as one. The end-wall limit itself, $2.5\ \mathrm{MW\,m^{-2}}$, is comparable to steady divertor targets in tokamak practice [21], so the expander brings a mirror end-loss problem into a regime with an established engineering answer.

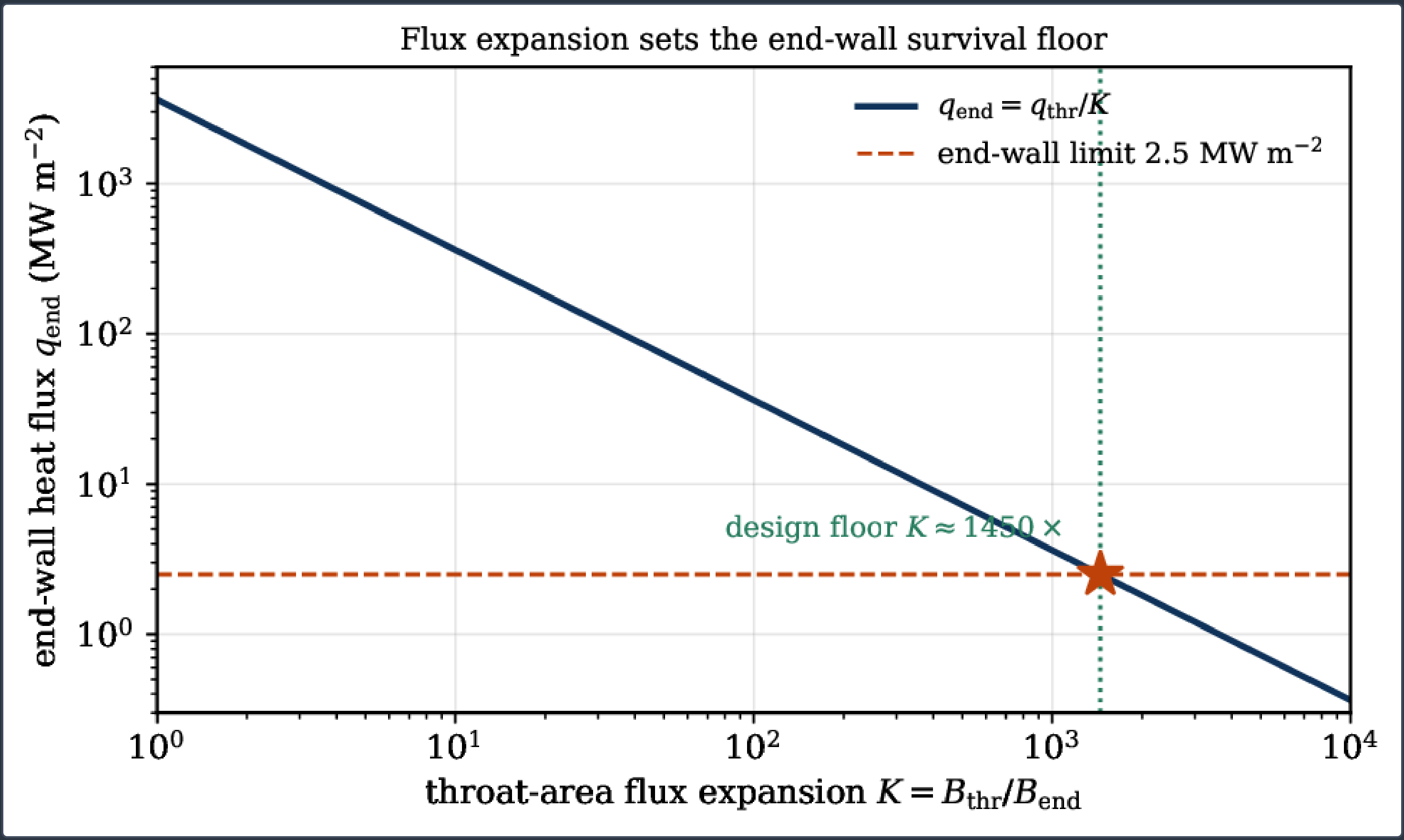

Expander flux-expansion floor (AG-CX-11). The end-wall heat flux $q_{\mathrm{end}} = q_{\mathrm{thr}}/K$ falls inversely with the throat-area expansion $K = B_{\mathrm{thr}}/B_{\mathrm{end}}$; the $2.5\ \mathrm{MW\,m^{-2}}$ limit (dashed) is reached at the design floor $K \approx 1450\times$ (star).

END-LOSS POWER HANDLING, THE DIRECT CONVERTER, AND THE HALO

Figure 8 closes the loss budget in power terms. At the 2.5 MW m^{-2} working flux the expander region carries ~ 816 MW, part of the ~ 3596 MW total thermal power handled in the MetroVolt housing (the first wall carrying the balance at a gentler 1.17 MW m^{-2}; serial MV-L1-A2). Of the axial charged-particle stream that reaches the converter, a fraction $\eta_{\mathrm{DEC}} = 0.49$ is recovered directly, without a thermal cycle, by an electrostatic decelerator whose venetian-blind lineage is classical [11] and whose collector and architecture details are treated in the companion papers [35]. The scrape-off/halo layer outside the core flux tube—the plasma that does not map cleanly onto the converter—is intercepted by a dedicated halo scraper so that the end-loss is handled within the wall limit. Four end controllers close these loops in the real-time control suite: the expander-region controller (KFE-CF-BU-011), the direct-converter collector optimizer (KFE-CF-BU-012), the halo-scraper controller (KFE-CF-BU-013), and the end-loss-ion recovery optimizer (KFE-CF-BU-014), each with an in-simulation acceptance test on its set-point [36] (Table 2).

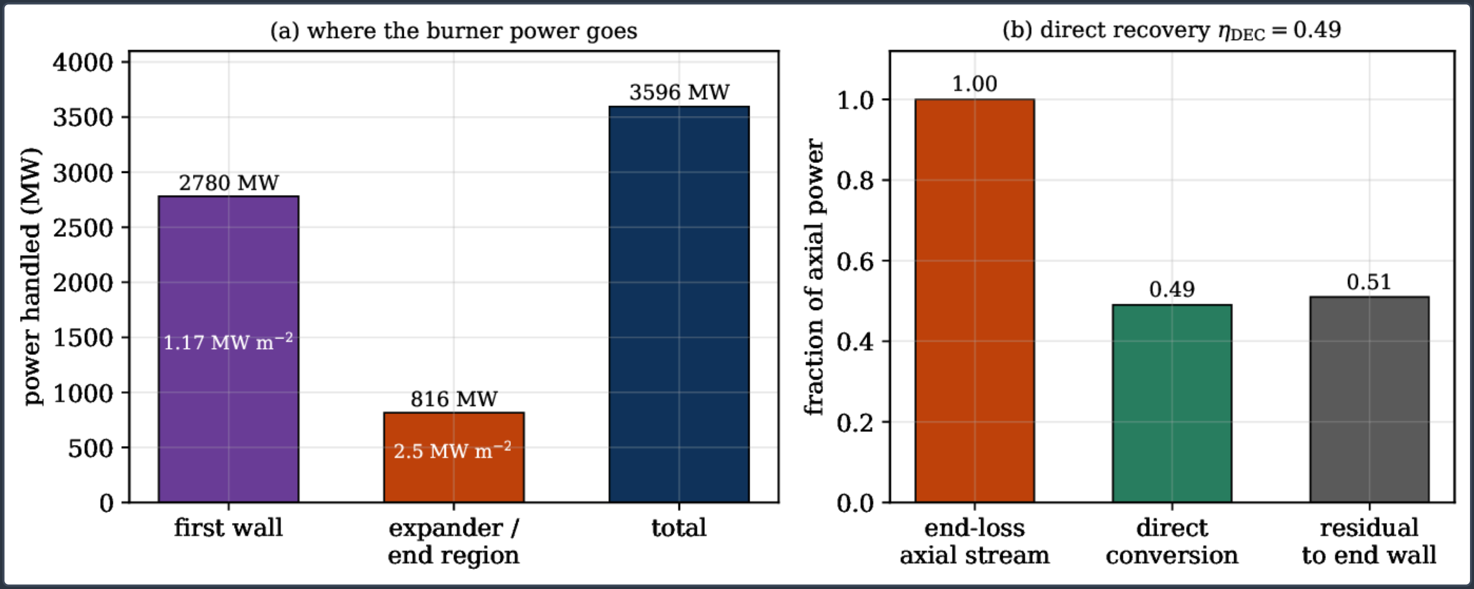

End-loss power handling (MV-L1-A2, BU-L1-A10, AG-CX-11). (a) The burner's thermal power is split between the first wall (~ 2780 MW at 1.17 MW m^{-2}) and the expander/end region (~ 816 MW at 2.5 MW m^{-2}). (b) The axial charged-particle stream is recovered directly at $\eta_{\mathrm{DEC}} = 0.49$, with the remainder handled thermally at the end wall.

CONTROLLER	FUNCTION	SERIAL
expander-region controller	holds expander state at set-point	KFE-CF-BU-011
direct-converter collector optimizer	maximizes recovered DEC efficiency	KFE-CF-BU-012
halo-scraper controller	keeps end-loss within the wall limit	KFE-CF-BU-013
end-loss-ion recovery optimizer	improves recovered ion fraction	KFE-CF-BU-014

The four end controllers that close the expander, direct-converter and halo loops in the real-time control suite [36]. Each carries an in-simulation acceptance test on its set-point.

THE ASSEMBLED END

Figure 9 assembles the pieces into the half-machine axial layout: the central cell at 5.50 T and $\beta_c = 0.55$; the sloshing/thermal-barrier plug rising to the 17 T throat behind the 26.49 T-on-conductor plug coil, with the twin off-midplane potential peaks; and the expander fanning the field out by $K \approx 1450\times$ to the end wall, where the direct converter and halo scraper recover and manage what leaves.

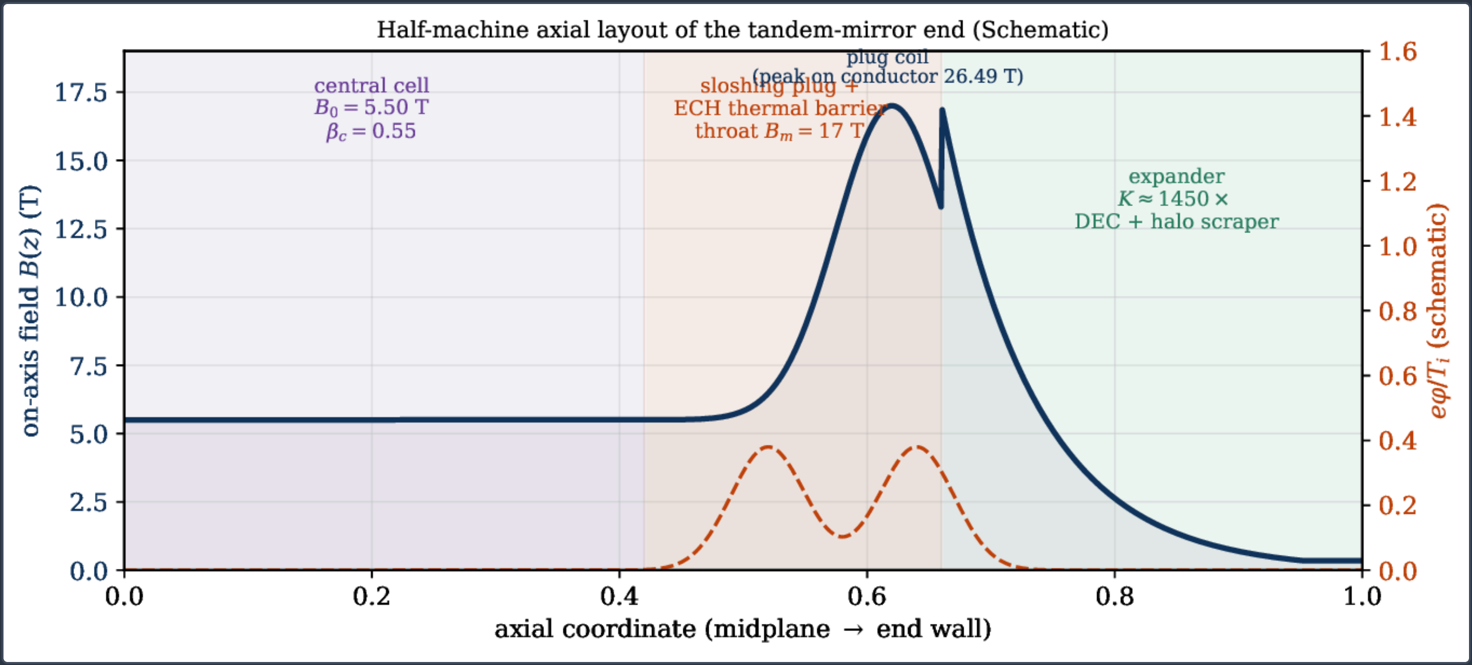

(Schematic.) Half-machine axial layout of the tandem-mirror end: on-axis field $B(z)$ (blue) rising from the 5.50 T central cell to the 17 T throat and fanning out in the expander, with the sloshing-ion confining potential (dashed orange, schematic) forming twin off-midplane peaks. The plug coil sees 26.49 T on conductor; the expander delivers $K \approx 1450\times$ flux expansion to the end wall, direct converter and halo scraper.

§ 5

Discussion

The ends are the confinement system, and each piece benchmarks against the mirror literature. The sloshing-ion plug reproduces the off-midplane density accumulation that Correll *et al.* produced in high-β mirror plasmas [10] and that the tandem-mirror concept requires [1]; our frozen well ($\Delta\varphi \approx 0.38\,T_i$ at $z/L_m \approx \pm 0.24$) is a specific, computed instance of that mechanism. The ECH thermal barrier follows directly the Baldwin–Logan prescription [3] whose production and identification were demonstrated in TMX-U [9]; our contribution is to quantify its worth at this operating point—a factor 2.8 in Q_E—which makes barrier reliability a design-driving criticality rather than a physics curiosity. The Pastukhov–Cohen confinement enhancement we use, Eq. (4), is the textbook result [6,7,8], applied without embellishment. The MHD margin is the most reassuring benchmark: $\beta_c = 0.55$ is a factor 1.82 below the hard $\beta = 1$ limit and essentially the value at which the gas-dynamic trap operates stably [13,15], and the interchange stabilization we invoke—min-B anchor plus energetic stabilizer—is the same physics as GDT vortex confinement and sloshing-ion stabilization [16]. The throat field the plug plasma sees, 17 T, is exactly WHAM's demonstrated HTS field [12], so the magnetic requirement is not an extrapolation. The expander brings the end-loss flux to 2.5 MW m^{-2}, comparable to steady tokamak divertor targets [21], and the direct converter that then recovers $\eta_{\mathrm{DEC}} = 0.49$ of the axial stream is the classical venetian-blind device [11]. Placed against the simpler-high-gain-tandem argument of Fowler, Moir and Simonen [17,18], the Kronos ends are a concrete, number-by-number realization of that program for a D–^{3}He burner rather than a D–T one, with the low neutron fraction ($f_n = 5.44\,\%$) that the advanced fuel buys [20].

§ 6

Limitations

The end-cell configuration is grounded in the WHAM axisymmetric mirror, whose 17 T HTS field and sloshing-ion stabilization it extends. The one open item is that the 90 keV ion temperature and the D–^{3}He burn are extrapolations beyond WHAM's present operating regime [12]: the confinement physics (Pastukhov–Cohen, thermal barrier, sloshing well) and the stability physics (min-B plus energetic stabilizer) are established, but the specific 90 keV, D–^{3}He anchors are provisional and are to be confirmed at commissioning. The reduced kinetic-orbit sloshing model and the 1-D hybrid-PIC stabilizer model are microstability- and orbit-channel calculations; a fully self-consistent multi-dimensional kinetic simulation of the coupled plug is a next-level verification, not a result claimed here.

§ 7

Conclusion

The Kronos burner's mirror ends are a designed, quantified confinement system at the frozen operating point, and they close the loss budget. A sloshing-ion plug forms an off-midplane confining well of $\Delta\varphi \approx +0.38\,T_i$ at $z/L_m \approx \pm 0.24$; an ECH thermal barrier holding the central electrons near 90 keV is worth a factor 2.8 in engineering gain; an energetic kinetic stabilizer quenches the residual end-cell mode for $f_s \gtrsim 0.30$, collapsing its amplitude from $145\times$ to $3\times$; the mirror ratio sits at the economic knee $R_{mc} \approx 4.6$, diamagnetically deepened from the vacuum $R_{\mathrm{vac}} = 3.09$ at $\beta_c = 0.55$; and the expander delivers the $\sim 1450\times$ flux expansion that holds the end wall at 2.5 MW m^{-2} while carrying ~ 816 MW, with a direct converter recovering $\eta_{\mathrm{DEC}} = 0.49$ of the axial stream and a halo scraper managing the scrape-off layer. Every number is the output of a written governing equation solved on the NVIDIA GPU HPC campaign and benchmarked against WHAM, GDT, TMX-U and the classical direct converter. Grounded in the WHAM 17 T HTS platform, with the breeder centrepost (16.84 T) and the burner plug (26.49 T) treated as the distinct magnets they are, the mirror ends are the confinement system that makes the D–^{3}He burner close.

Acknowledgments tocsectionAcknowledgments Part of the Kronos Fusion Energy 2026 design series. The authors thank the Kronos physics de-risking programme for the frozen result set underlying every quantitative claim, and acknowledge the NVIDIA GPU HPC campaign on which the end-cell, mirror-ratio and expander calculations were run.

Reproducibility. The end-cell, mirror-ratio and expander values are frozen results (AG-CX-01, AG-CX-03, AG-CX-05, AG-CX-06, AG-CX-11, AG-DR-03, KX-L1-A18-BU, BU-L1-A2, BU-L1-A10, MV-L1-A2) in the Kronos Physics De-Risking Register, doi:10.5281/zenodo.22133057. This paper is archived at its DOI doi:10.5281/zenodo.22645852; official version: https://www.kronosfusionenergy.com/publications/end-cell-expander-and-halo-physics-in-a-d-3he-tandem-mi.html and its official page https://www.kronosfusionenergy.com/publications/end-cell-expander-and-halo-physics-in-a-d-3he-tandem-mi.html; the register is doi:10.5281/zenodo.22133057. The kinetic-orbit and hybrid-PIC inputs and the single figure-generation script (`make_endcell_2-59_figs.py`) are archived with the deposit and reference the Kronos 2026 series and its Physics De-Risking Register.

Data availability tocsectionData availability The sloshing-potential, stabilizer, mirror-ratio, thermal-barrier, Pastukhov, β-margin, expander and power-handling values used for Figures 1–9 are archived with the deposit at doi:10.5281/zenodo.22645852, which references the Kronos 2026 series including the AI and quantum-control paper [37]. All quantitative values trace to the register [28] by the serial identifiers cited inline. Any economic analysis is reported separately and is not part of the public deposit.

Competing interests tocsectionCompeting interests Provisional patent applications relating to aspects of this work have been filed. The authors declare no other competing interests.

tocsectionReferences

APPARATUS

Portfolio, People & Record

The intellectual-property estate, the people who built it, the limitations that gate it, and the sources it rests on.

1	4	40	27
GRANTED PATENT	2026 PROVISIONALS	TEAM MEMBERS	2022 PROVISIONALS

INTELLECTUAL PROPERTY

The patent portfolio

The estate spans a granted high-field magnet patent, pending utility and 2026 provisional filings that map to the two products, a digital-twin control provisional, a registered trademark application, and the original 2022 provisional family. Every patentable disclosure in the five-paper arXiv drop was protected **before** publication: the breeder and burner provisionals were filed 1–2 August, and a publication-gap omnibus filing the evening before the drop swept up the DEC, plasma-control, and REBCO-winding matter of the three otherwise-unprotected papers. Patent numbers and application serials are matters of public record; claim scope is summarised, not reproduced.

GRANTED & PENDING UTILITY

US 12,009,112	High-field tilted graded-REBCO magnet architecture (KRONO-002A) · *app. 17/878,550*	GRANTED
US 17/878,507	Core device / method (KRONO-001A) · *utility*	PENDING

2026 PROVISIONAL FILINGS — MAPPED TO THE PRODUCTS

64/124,209	Hyperion — spherical-tokamak tritium / helium-3 foundry · *breeder · filed Aug 2026*	FILED
64/124,220	Aegis / MetroVolt — synchrotron-cutoff, fuel-selection & plug-winding · *generator · filed Aug 2026*	FILED
64/115,167	KRONOS-CTRL digital-twin plant control · *provisional · filed Jul 2026*	FILED
64/005,440	Integrated spherical-tokamak fusion architecture · *early integrated-architecture filing · filed Mar 2026*	FILED
64/105,530	Negative-triangularity spherical-tokamak architecture · *foundational ST filing · filed Jul 2026*	FILED
64/128,097	Publication-gap omnibus — quasineutral two-species expander DEC · provenance-gated / latency-split plasma control · as-built high-field winding & conductor architecture · *filed 7 Aug 2026, the evening before the arXiv drop*	FILED

TRADEMARK & ORIGIN

FTK-98801894	Kronos Fusion Energy — trademark application	FILED
KR-2022-*	Original provisional family (KR-2022-00001 … 00027) · *27 filings, 2022*	PRIORITY

The narrow, defensible magnet novelty — the specific conductor and the digital-twin winding optimisation, not high-field REBCO as a category — is the commercial core that can earn ahead of any Q > 1 milestone, with markets in fusion magnet supply, MRI/NMR, accelerators, and proton therapy. The claim is scoped honestly: the high field is a *system field* result, not a stand-alone-coil record; the small-bore plug coil is structurally infeasible as a bare winding but resolved by a stress-managed structural shield (feasible-pending-FEA); and the winding-tape experiment returned a *null result*. The value is the method, not a field record.

THE TEAM

Founding partners, board, advisors & auditors

Kronos is built by a bench of advanced-fuel-fusion, high-field-magnet, direct-conversion, and materials specialists, with a board and operations team drawn from defense, national laboratories, and industry. Dates are shown as ranges; where a tenure has ended or is term-ending, the range says so.

FOUNDING PARTNERS — SCIENCE

Dr. Gerald Kulcinski
Co-Founder · Helium-3 & Advanced-Fuel Fusion
UW–Madison · 2023–Present

Dr. Carl Weggel
Chief Scientist / S.M.A.R.T. Design
MIT Alcator Program · 2022–Present

Dr. Robert J. Weggel
Magnetic Field Design
MIT Magnet Lab · 2022–Present

BOARD

Priyanca Ford
Founder & CEO · Executive Board
2022–Present

Bandel Carano
Finance / Strategy
Oak Investment Partners / Stanford · 2025–2026

Patrick Schweiger
Fusion Device Engineering
Oklo / CFS / TerraPower · 2025–Present

SCIENTIFIC ADVISORS

Dr. Steven O. Dean
Fusion Policy & History
DOE / Fusion Power Associates · 2025–Present

Dr. Patrick H. Diamond
Plasma Turbulence & Transport
UC San Diego · 2025–Present

Dr. Jack J. Dongarra
HPC & Numerical Algorithms
Turing Award · 2025–Present

Dr. Nasr M. Ghoniem
Chief Material Scientist
UCLA · 2025–Present

Dr. Siegfried Glenzer
Plasma Physics & Laser Fusion
Stanford / SLAC · 2022–Present

Dr. David A. Hammer
Pulsed-Power Fusion
Cornell · 2025–Present

Dr. Donald A. Spong
Plasma Theory & Confinement
ORNL · 2025–Present

Dr. Curtis Smith
Risk Assessment & Nuclear PRA
MIT / Idaho National Lab · 2025–Present

RADM (Ret.) David Goggins
Naval Engineering & Power-Plant Design
U.S. Navy · 2023–2026

Dr. Konstantin Batygin
Mathematician
Caltech · 2022–2025

Dr. Ruben Fair
Magnet Design / ITER Liaison
PPPL / Jefferson Lab · 2022–2025

Dr. Paul S. Weiss
Materials & Nanotechnology
UCLA · 2022–2025

SCIENTIFIC AUDITORS

Dr. Wilfred A. Cooper
Plasma Equilibrium Theory
EPFL / Swiss Plasma Center · 2025–Present

Dr. Ahmed Hassanein
Plasma–Material Interactions
Purdue / Argonne · 2025–Present

Dr. Patrick E. Hopkins
Extreme Thermal Materials
U. of Virginia · 2025–Present

Dr. Peter Hosemann
Materials Joining & Structural Integrity
UC Berkeley · 2025–Present

Dr. Travis W. Knight
Advanced Nuclear Fuels & Systems
U. of South Carolina · 2025–Present

Dr. Philippe Lebrun
Cryogenics & Magnet Cooling
CERN · 2025–Present

Dr. Nitendra Singh
Nuclear Safety & Fuel Cycle
ITER · 2025–Present

Dr. Guido Van Oost
Magnetic Confinement & Fusion Systems
Ghent University · 2025–Present

Dr. Gary S. Was
Radiation Materials & Structural Integrity
U. of Michigan · 2025–Present

Dr. Ray Sedwick
Direct Energy Conversion
U. of Maryland · 2025

OPERATIONS

Michael Laughlin
Chief Operating Officer
2022–Present

Martin Owens
Chief Strategy Officer
LANL / GE Hitachi · 2022–Present

MG (Ret.) Paul Pardew
Chief Contracting Officer
Army Contracting Command · 2022–Present

David Beck
Fusion Commercialization
U.S. Space Force · 2024–Present

Sushma Bhatia
Environmental & Legislative
Google · 2022–Present

Michael De Frenza
Technology Licensing
2023–Present

MG (Ret.) Robin L. Fontes
Cybersecurity & Defense
Army Cyber Command · 2022–Present

Vijay Gehani
Supply Chain & Components
INOX India · 2024–Present

Jon Michel Greenwood
IT & AI Infrastructure
Live Nation · 2023–Present

Brian C. O'Neill
National Security
CIA / ODNI · 2022–Present

Gen. (Ret.) Gustave F. Perna
DoD Liaison
Operation Warp Speed · 2022–2023

Andrea Romero
Marketing Lead
2022–Present

Legal counsel is retained; those roles are held on the internal roster and are not listed here.

SOURCES

References

1 G I Dimov, V V Zakaidakov and M E Kishinevsky, Thermonuclear confinement with twin mirror systems, *Sov. J. Plasma Phys.* **2** 326 (1976).

2 T K Fowler and B G Logan, The tandem mirror reactor, *Comments Plasma Phys. Control. Fusion* **2** 167 (1977).

3 D E Baldwin and B G Logan, Improved tandem mirror fusion reactor, *Phys. Rev. Lett.* **43** 1318 (1979). doi:10.1103/PhysRevLett.43.1318

4 D E Baldwin, End-loss processes from mirror machines, *Rev. Mod. Phys.* **49** 317 (1977). doi:10.1103/RevModPhys.49.317

5 R F Post, The magnetic mirror approach to fusion, *Nucl. Fusion* **27** 1579 (1987). doi:10.1088/0029-5515/27/10/001

6 V P Pastukhov, Collisional losses of electrons from an adiabatic trap in a plasma with a positive potential, *Nucl. Fusion* **14** 3 (1974). doi:10.1088/0029-5515/14/1/001

7 R H Cohen, M E Rensink, T A Cutler and A A Mirin, Collisional loss of electrostatically confined species in a magnetic mirror, *Nucl. Fusion* **18** 1229 (1978). doi:10.1088/0029-5515/18/9/005

8 T D Rognlien and T A Cutler, Transition from Pastukhov to collisional confinement in a magnetic and electrostatic well, *Nucl. Fusion* **20** 1003 (1980). doi:10.1088/0029-5515/20/8/007

9 D P Grubb *et al*, Thermal-barrier production and identification in a tandem mirror, *Phys. Rev. Lett.* **53** 783 (1984). doi:10.1103/PhysRevLett.53.783

10 D L Correll *et al*, Production of large-radius, high-beta, confined mirror plasmas, *Nucl. Fusion* **20** 655 (1980). doi:10.1088/0029-5515/20/6/001

11 R W Moir and W L Barr, "Venetian-blind" direct energy converter for fusion reactors, *Nucl. Fusion* **13** 35 (1973). doi:10.1088/0029-5515/13/1/005

12 D Endrizzi *et al*, Physics basis for the Wisconsin HTS Axisymmetric Mirror (WHAM), *J. Plasma Phys.* **89** 975890501 (2023). doi:10.1017/S0022377823000806

13 A A Ivanov and V V Prikhodko, Gas-dynamic trap: an overview of the concept and experimental results, *Plasma Phys. Control. Fusion* **55** 063001 (2013). doi:10.1088/0741-3335/55/6/063001

14 A A Ivanov and V V Prikhodko, Gas dynamic trap: experimental results and future prospects, *Phys.-Usp.* **60** 509 (2017). doi:10.3367/UFNe.2016.09.037967

15 P A Bagryansky *et al*, Threefold increase of the bulk electron temperature of plasma discharges in a magnetic mirror device, *Phys. Rev. Lett.* **114** 205001 (2015). doi:10.1103/PhysRevLett.114.205001

16 A D Beklemishev, P A Bagryansky, M S Chaschin and E I Soldatkina, Vortex confinement of plasmas in symmetric mirror traps, *Fusion Sci. Technol.* **57** 351 (2010). doi:10.13182/FST10-A9497

17 T K Fowler, R W Moir and T C Simonen, A new simpler way to obtain high fusion power gain in tandem mirrors, *Nucl. Fusion* **57** 092001 (2017). doi:10.1088/1741-4326/aa5e54

18 T C Simonen *et al*, Three game changing discoveries: a simpler fusion concept?, *J. Fusion Energy* **35** 63 (2016). doi:10.1007/s10894-015-0017-2

19 H-S Bosch and G M Hale, Improved formulas for fusion cross-sections and thermal reactivities, *Nucl. Fusion* **32** 611 (1992). doi:10.1088/0029-5515/32/4/I07

20 L J Wittenberg, J F Santarius and G L Kulcinski, Lunar source of ^{3}He for commercial fusion power, *Fusion Technol.* **10** 167 (1986). doi:10.13182/FST86-A24972

21 R A Pitts *et al*, A full tungsten divertor for ITER: physics issues and design status, *J. Nucl. Mater.* **438** S48 (2013). doi:10.1016/j.jnucmat.2013.01.008

22 G M Staebler, J E Kinsey and R E Waltz, A theory-based transport model with comprehensive physics, *Phys. Plasmas* **14** 055909 (2007). doi:10.1063/1.2436852

COLOPHON

How this document was made

The Kronos Fleet — Combined Editorial, 2026 is set in **Fraunces** (display), **Gelasio** (text), and **IBM Plex Mono** (data & equations), carried forward from the Kronos editorial design system.

The figures are rendered at 300 dpi from the deposited generator scripts; the document is composed as a single self-contained file with embedded fonts and imagery, paginated to US Letter, and rendered to PDF through a headless Chromium engine in matched light and dark editions.

Every headline quantity carries an evidence class; withdrawn and restated values are marked as such. Nothing herein is frozen beyond the founder-approved Tier-A set.

Explore it live — turn the interactive 3-D model, run the deposited solvers in the physics validator, and watch the companion film series.

LEGAL NOTICE

Notice, status, and distribution

Conceptual design & simulation study. This document reports a conceptual design and simulation study. It is not a construction commitment, a safety-analysis report, a regulatory filing, or an offer of securities. Forward-looking statements — schedules, costs, market sizes, and performance — are estimates subject to the limitations set out in the Simulations part and may change.

Numbers and their classes. Quantities are reported with evidence classes and case labels; modelled, assumed, and requirement-class values are identified as such and are not to be quoted without their labels.

Public edition. This edition carries the physics and design only; all financial, funding, and defense-commercial content has been removed for public distribution. The scientific text corresponds to the arXiv and journal submissions.

THE 2026 KRONOS SERIES

One programme, many papers

This editorial is one paper in the Kronos 2026 series — a real fusion company's complete, reproducible physics record for a spherical-tokamak breeder and its low-neutron D–^{3}He tandem-mirror burners. Every headline number is a frozen anchor in the Physics De-Risking Register.

Explore the whole programme: the De-Risking Register, the interactive 3-D model, and the physics validator.

KRONOS FUSION ENERGY

End-Cell, Expander, and Halo Physics in a D-3He Tandem-Mirror Burner: The Mirror Ends That Set the Loss Budget

A real fusion company building real machines. Explore the science, live.

Zenodo · doi:10.5281/zenodo.22645852

Read on kronosfusionenergy.com

The Physics De-Risking Register